peratures of ~11° to 13°C, though seasonal temperature variability is unclear (*14, 23*). Physiological models for a 5000-kg bradymetabolic hadrosaur predict that annual core body temperature variation would be large (~20°C, which is equivalent to a 4.5 per mil δ_p variation) in a simulated Cretaceous environment, though monthly temperature variability would be small (1° to 3°C) (*24*). A minimum isotopic variability of 3.5 per mil (15°C) is suggested even if individuals were capable of always maintaining body temperatures above 20°C, the minimum temperature at which most extant ectotherms can digest food. Because of its similar size (~6000 kg) (*14*), temperature variability should be similar in a bradymetabolic *Tyrannosaurus*. The small intrabone δ_p variation indicates that this *T. rex* was not an ectotherm. The lack of increased intrabone variation in the limbs and tail and the small interbone variation suggest that this *T. rex* was also not a mass homeotherm using heat exchange mechanisms to dump heat through the extremities during warm periods and retain core body heat during colder periods. However, if it can be shown that there was little seasonal temperature variability (that is, less than 8° to 10°C) during early Hell Creek time, then mass homeothermy remains a valid interpretation of the data.

Because this *T. rex* does not have either large intrabone or interbone δ_p variability, we conclude that it was a nonmigratory endotherm. The metabolism of *T. rex* may or may not have been as high as that of modern endotherms, but it was high enough that body temperatures were largely maintained by a controlled metabolic rate, unlike the metabolism of modern ectotherms. The difference in metabolic rates for ectotherms and endotherms narrows at larger sizes (*25*), but the difference is still important when extrapolated to weights of 6 or 7 tons. It is therefore likely that *Tyrannosaurus* metabolic rates were closer to those of a modern 6-ton endotherm (such as a bull African elephant) than to those of a postulated 6-ton ectotherm. Metabolic rates may, however, have undergone seasonal shifts (*2*) in order to maintain homeothermy. Endothermy would have allowed tyrannosaurs the aerobic stamina (*26*) to be active predators or scavengers (or both) that were independent of ambient temperature fluctuations.

REFERENCES AND NOTES

1. R. R. Rogers *et al.*, *Science* **260**, 794 (1993).
2. J. O. Farlow, in *The Dinosauria*, D. Weishampel, P. Dodson, H. Osmolska, Eds. (Univ. of California Press, Berkeley, CA, 1990), pp. 43–55.
3. J. Bligh and K. G. Johnson, *J. Appl. Physiol.* **35**, 941 (1973).
4. A. Longinelli and S. Nuti, *Earth Planet. Sci. Lett.* **19**, 373 (1973).
5. Y. Kolodny, B. Luz, O. Navon, *ibid.* **64**, 398 (1983).
6. B. Luz and Y. Kolodny, *Appl. Geochem.* **4**, 317 (1989).
7. A. Longinelli, *Geochim. Cosmochim. Acta* **48**, 385 (1984).
8. B. Luz, Y. Kolodny, J. Kovach, *Earth Planet. Sci. Lett.* **69**, 255 (1984).
9. B. Luz and Y. Kolodny, *ibid.* **75**, 29 (1985).
10. B. Luz, A. B. Cormi, H. P. Schwarcz, *Geochim. Cosmochim. Acta* **54**, 1723 (1990); D. D'Angela and A. Longinelli, *Chem. Geol.* **86**, 75 (1990); N. Yoshida and N. Miyazaki, *J. Geophys. Res.* **96**, 815 (1991).
11. $$\delta^{18}O = \left(\frac{{}^{18/16}O_{sample}/{}^{18/16}O_{standard}}{{}^{18/16}O_{standard}} \right) \times 1000$$
The standard used is standard mean ocean water (SMOW).
12. K. P. Pflug, K. D. Schuster, J. P. Pichotka, H. Forstel, in *Stable Isotopes: Proceedings of the Third International Conference*, Oak Brook, IL, 23 to 26 May 1978, E. R. Klein and P. D. Klein, Eds. (Academic Press, New York, 1979), pp. 553–561; D. A. Schoeller *et al.*, *Am. J. Physiol.* **251**, 1137 (1986); W. W. Wong *et al.*, *Am. J. Clin. Nutr.* **47**, 1 (1988).
13. The *T. rex* bone samples were obtained from a specimen that was collected in the Maastrichtian Hell Creek Formation in McCone County, MT, and is now in the Museum of the Rockies, Bozeman, MT (MOR 555). We collected powder samples by drilling one or two holes into each bone. Powder was collected at several intervals within the holes in order to sample a cross-section of bone that included both compact and cancellous bone. Samples were isotopically analyzed following the technique of R. C. Crowson, W. J. Showers, E. K. Wright, and T. C. Hoering [*Anal. Chem.* **63**, 2397 (1991)]. The results are reported in per mil deviations from SMOW. The NBS 120c standard has an analytical precision of 0.07 per mil with this $\delta^{18}O\text{-}PO_4$ technique. Calcite cements were isotopically analyzed by reacting the samples for 5 min at 90°C in 100% orthophosphoric acid. Structural CO_3 was isotopically analyzed by the method of Y. Kolodny and I. R. Kaplan [*J. Sediment Petrol.* **40**, 954 (1970)]. Samples were leached in a weak acetic acid solution [S. R. Silverman, R. K. Fugat, J. D. Weiser, *Am. Mineral.* **37**, 211 (1952)] for 3 days, washed, and then reacted for 4 hours at 90°C in 100% orthophosphoric acid. The resultant CO_2 from both procedures was cryogenically purified and then analyzed in a Finnigan MAT 251 ratio mass spectrometer (Finnegan MAT, Bremen, Germany). The machine standard was calibrated against the NBS 19 standard and the results are reported in per mil deviations from the Pee Dee belemnite standard.
14. J. R. Horner and D. Lessem, *The Complete* T. rex (Simon and Schuster, New York, 1993).
15. H. Francillon-Vieillot *et al.*, in *Skeletal Biomineralization*, J. G. Carter, Ed. (Van Nostrand Reinhold, New York, 1990), pp. 471–530.
16. A. N. Garland, in *Science and Archaeology*, E. A. Slater and J. O. Tate, Eds. (British Archaeological Reports, Oxford, 1988), pp. 321–338.
17. H. M. Frost, in *Fundamental and Clinical Bone Physiology*, M. R. Urist, Ed. (Lippincott, Philadelphia, 1980), pp. 208–241.
18. W. F. Neuman and M. W. Neuman, *The Chemical Dynamics of Bone Mineral* (Univ. of Chicago Press, Chicago, 1958); J. H. Marshall *et al.*, *Health Phys.* **24**, 125 (1973); G. I. Tanaka, H. Kawamura, E. Nomura, *ibid.* **40**, 601 (1981).
19. F. V. Paladino, M. P. O'Connor, J. R. Spotila, *Nature* **344**, 858 (1989).
20. J. R. Spotila, M. P. O'Connor, P. Dodson, F. V. Paladino, *Mod. Geol.* **16**, 203 (1991); J. R. Spotila, P. Lommen, G. S. Bakken, D. M. Gates, *Am. Nat.* **107**, 391 (1973).
21. T. Crowely and G. North, *Paleoclimatology* (Oxford Univ. Press, Oxford, 1991).
22. E. Barron and W. Washington, *Palaeogeogr. Palaeoclimatol. Palaeoecol.* **40**, 103 (1982).
23. K. R. Johnson and L. J. Hickey, *Geol. Soc. Am. Spec. Pap.* **247**, 433 (1990).
24. A. E. Dunham, K. L. Overall, W. P. Porter, C. A. Forster, *ibid.* **238**, 1 (1980).
25. K. A. Nagy, *Ecol. Monogr.* **57**, 111 (1987); B. McNab, *J. Zool.* **199**, 1 (1983).
26. A. F. Bennett and J. A. Ruben, *Science* **206**, 649 (1979).

27. We wish to thank M. Stoskopf, M. Bevis, D. DeMaster, and two anonymous reviewers for reviewing this article and J. Horner for assistance in collecting samples. A. Fischer generously provided ideas and enthusiasm. Supported by NSF grant EAR91-06660.

7 March 1994; accepted 16 May 1994

The Role of the Tropical Super Greenhouse Effect in Heating the Ocean Surface

Dan Lubin

Measurements made by a Fourier transform infrared (FTIR) spectroradiometer operating in the middle infrared (5 to 20 micrometers, with a spectral resolution of one inverse centimeter) imply that there is an anomalously large greenhouse effect over equatorial oceans that is caused by water vapor. As sea-surface temperature increased from 297 to 303 degrees kelvin, the net infrared cooling at the surface decreased by 30 to 50 watts per square meter. Thus, according to the FTIR data, the super greenhouse effect that had been inferred from satellite measurements contributes directly to radiative heating of the sea surface. The data demonstrate that most of this heating occurs in the middle infrared by means of the continuum emission window of water vapor and that tropical deep convection contributes substantially to this super greenhouse effect.

The western tropical Pacific Ocean has the hottest sea-surface temperatures and the largest burden of tropospheric water vapor in the world. Thus, greenhouse forcing by water vapor might be expected to be greatest there. Two major international experiments were conducted from late 1992 to early 1993 (*1*), whose object was to evaluate the climate feedbacks in the region.

In the western tropical Pacific, sea-surface temperature rarely exceeds 303 K (*2*). This upper limit is most apparent in regions of extensive convection (*3*). Ramanthan and

California Space Institute and Center for Clouds, Chemistry, and Climate, University of California, San Diego, La Jolla, CA 92093–0221, USA.

Collins (4) have proposed a self-regulating mechanism whereby the anvil cirrus clouds that result from deep convection attenuate the solar energy input to the ocean surface, thereby allowing the tropical atmosphere to cool and limit maximum sea-surface temperatures. A critical component of their hypothesis is the so-called super greenhouse effect (5). At high sea-surface temperatures, the longwave energy trapped by the atmospheric column, G_a (6), increases with sea-surface temperature at a faster rate than does the blackbody surface radiation. Water vapor is the most important greenhouse gas, and the super greenhouse effect is caused by large increases in water vapor (as sea-surface temperature increases) and the subsequent trapping of infrared radiation. This radiative process is augmented by tropical deep convection, which gives rise to large abundances of tropospheric water vapor. These processes, combined with enhanced tropospheric lapse rates, which occur in regions of deep convection, result in a nonlinear increase in greenhouse trapping by the atmosphere at the highest sea-surface temperatures. Here I present results from the Central Equatorial Pacific Experiment (CEPEX) (1) that quantify the degree to which the super greenhouse effect heats the atmosphere and the sea surface.

Satellite measurements have demonstrated that a super greenhouse effect develops at sea-surface temperatures greater than 300 K (Fig. 1). Satellite data indicate that the super greenhouse effect consists of two factors: (i) There is a nonlinear increase in G_a at high sea-surface temperatures. (ii) The rate of increase of G_a with sea-surface temperature exceeds the rate of increase of blackbody radiation with sea-surface temperature. The existence of the super greenhouse effect has been shown to be independent of the tropical ocean basin (7), independent of season and hemisphere (8), and independent of the year (4). The super greenhouse effect was demonstrated by measurements made with aircraft-borne radiometers at the tropopause, during the time in which the CEPEX study was done (9). Although the super greenhouse effect has been extensively verified above the troposphere, it has not been shown whether this phenomenon results in a longwave back-radiation that contributes directly to local surface heating over the warm oceans. Unlike Venus, the Earth is not uniformly blanketed by a convectively driven super greenhouse effect. It is conceivable that longwave energy emitted by the warmer sea surface might be immediately advected to the adjacent nonconvective colder regions, in which case the primary role of the terrestrial super greenhouse effect would be to heat the troposphere (10).

As part of CEPEX, a Fourier transform infrared (FTIR) spectroradiometer was deployed aboard the R.V. *John Vickers*, which made a Pacific Ocean cruise beginning at Honiara in the Solomon Islands on 7 March 1993. The FTIR spectroradiometer (11–13) measured spectral radiance coming from the sky's zenith throughout the middle infrared (IR) wavelength range of 5 to 20 μm (500 to 2000 cm^{-1}), with a resolution of 1 cm^{-1}. The National Institute of Standards and Technology (NIST)–traceable radiometric calibration was established by a Mikron 340 blackbody source, after the method of Revercomb *et al.* (14). From these measurements of spectral radiance from the zenith, downwelling longwave flux can be estimated with the use of Gaussian quadrature (15).

In the first half of the CEPEX cruise, the ship proceeded from Honiara east along latitude 2°S, until due south of Christmas Island (2°N203°E, Republic of Kiribati), at which point the ship headed due north to that island. In the second half of the cruise, the ship moved due east along the latitude 2°N as far as longitude 213°E, at which point the ship turned northeast on a direct heading to Los Angeles. This cruise crossed four meteorological regions. The region between 174°E and 180°E was a convective warm pool region (4) with active deep convection. The region between 180°W and 164°W was part of the warm pool region, but convection was suppressed during the ship's transit. Between 164°W and 144°W, deep convection became active again, and during 1993 this region was also considered to be part of the convective warm pool. From 144°W to 120°W, the ship passed through the cooler eastern Pacific, throughout which convection was minimal. The properties of these four distinct regions

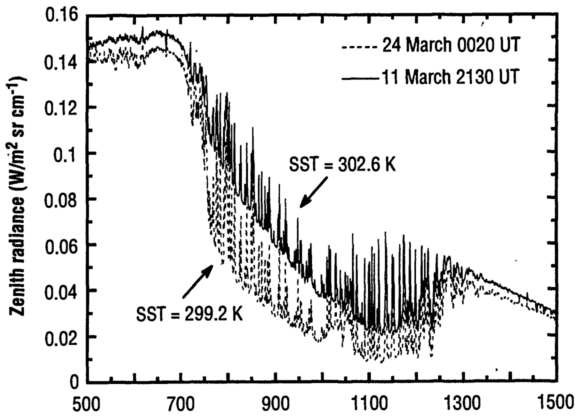

Fig. 2. Examples of atmospheric emission spectra measured by the FTIR spectroradiometer during CEPEX. The upper (solid) curve was recorded on 11 March 1993 (2130 UT) at 2°S 178°E, within the western Pacific warm pool region, where the sea-surface temperature (SST) was 302.6 K. The lower (dotted) curve was recorded on 24 March 1993 (0020 UT) at 12°N 138°W, outside of the warm pool region, where the sea-surface temperature was 299.2 K. Both spectra show the H_2O rotation lines (500 to 625 cm^{-1}), the emission band of CO_2 (625 to 675 cm^{-1}), the H_2O emission features and continuum (800 to 1250 cm^{-1}), the ozone emission band (1000 to 1080 cm^{-1}), and the water vapor vibration band (1250 to 1500 cm^{-1}).

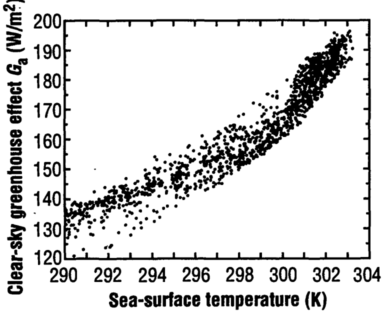

Fig. 1. Example of the clear-sky longwave greenhouse effect G_a, plotted versus sea-surface temperature, as measured at the top of the atmosphere by the Earth Radiation Budget Experiment (*4, 20*). Data are from March 1987 over the Pacific Ocean between 40°N and 40°S.

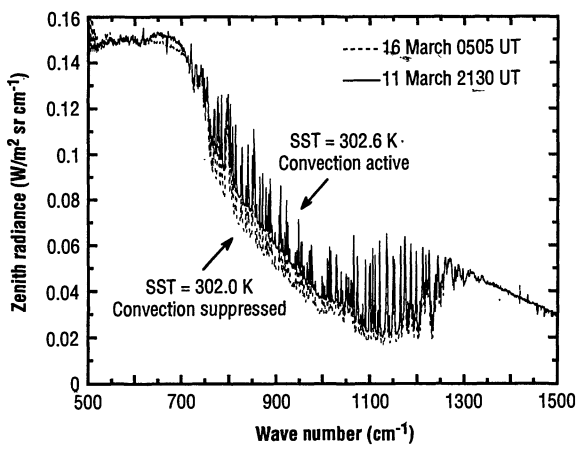

Fig. 3. Examples of atmospheric emission spectra measured within the warm pool by the FTIR spectroradiometer during CEPEX. The upper (solid) curve was recorded on 11 March 1993 (2130 UT) at 2°S 178°E, in a region of active convection. The lower (dotted) curve was recorded on 16 March 1993 (0505 UT) at 2°S 166°W in a region of suppressed convection. Rawindsondes on the *Vickers* indicated precipitable column abundances of H_2O vapor of 4.89 cm and 3.76 cm for 11 March and 16 March, respectively.

were documented by data from rawindsondes launched daily from the *Vickers*, by lidars deployed aboard the *Vickers*, and by meteorological radar (*16*).

The FTIR data were obtained when the instrument's field of view was entirely cloud-free, as observed visually throughout the time of measurement integration. A comparison of spectra obtained (for examples, see Fig. 2) with the MODTRAN 2 radiative transfer model (*15*) shows that all of the emission features measurable at a resolution of 1 cm^{-1} are accounted for in current atmospheric radiation databases (*17*). Differences between radiance measurements in the CO_2 and H_2O vibration bands are due to differences in temperature in the lower troposphere. For the study of climate, the most important difference between spectra lies in the mid-IR window (800 to 1250 cm^{-1}), where the major atmospheric emission is from the H_2O continuum. Zenith radiances from 800 to 1250 cm^{-1} are larger by up to a factor of 2 for the warm pool spectra than for spectra measured outside of the warm pool. This observation holds in general. The integrated radiance over the most transparent part of the mid-IR window (800 to 1000 cm^{-1}) was an average of 12.84 W/m^2 sr, with a standard deviation of 1.14 W/m^2 sr, for all spectra recorded when the sea-surface temperature exceeded 300 K. For all spectra recorded when the sea-surface temperature was less than 300 K, this integrated radiance was an average of 7.54 W/m^2 sr, with a standard deviation of 1.07 W/m^2 sr.

Within the warm pool region, mid-IR window radiances recorded in convective areas were typically 15% greater than those recorded in areas in which convection was suppressed (Fig. 3). For all spectra recorded between 180°W and 164°W, the integrated radiance in the interval from 800 to 1000 cm^{-1} was an average of 11.57 W/m^2 sr, with a standard deviation of 0.37 W/m^2 sr. For all other spectra recorded when the sea-surface temperature exceeded 300 K, this integrated radiance was an average of 13.43 W/m^2 sr, with a standard deviation of 0.86 W/m^2 sr. This additional surface radiance results when deep convection pumps additional water vapor into the troposphere, and it represents a typical surface flux enhancement of 13 W/m^2 for the convective areas relative to the areas of suppressed convection. From the vantage point of the ocean surface, haze and thin cirrus can be ruled out as substantial contributors to the measured longwave radiances. For reasonable estimates of visibility along the cruise track, a MODTRAN 2 calculation shows that maritime aerosols should add no more than 0.5 mW/m^2 sr cm^{-1} to the spectral radiance from the zenith in the mid-IR. Because of the great opacity of water vapor, sub-visible cirrus has a negligible impact on mid-IR radiance measured at the surface, although this may not be generally true for upwelling radiation measured at the tropopause.

These FTIR data may be used to estimate the net flux $F_n = F_u - F_d$ at the ocean surface, which is a measure of greenhouse trapping by the atmosphere. The smaller the net flux F_n, the more longwave surface energy is trapped by the atmosphere and radiated back to the surface. I transformed the FTIR measurements to a flux integral (*15*) over the measurable bandwidth from 5 to 20 μm. This bandwidth contains 70% of atmospheric longwave radiation (*18*). Upwelling flux was estimated from sea-surface temperatures T_s, logged by the *Vickers* as $F_u = \int_{\Delta\nu} B_\nu(T_s)d\nu$ where $B_\nu(T_s)$ is the Planck function evaluated at wave number ν, and $\Delta\nu$ refers to integration limits of 500 to 2000 cm^{-1}. With this bandwidth, $F_u \approx 0.72\sigma T^4$, where the Stefan-Boltzmann constant $\sigma = 5.67 \times 10^{-8}$ W m^{-2} K^{-4} (Fig. 4). The sea-surface emission in the bandwidth from 5 to 20 μm increased at a rate of approximately $dF_u/dT_s \approx 4.9$ W m^{-2} K^{-1}. For sea-surface temperatures less than 300 K, the downwelling flux increased at a slightly higher rate $dF_d/dT_s \approx 5.7$ W m^{-2} K^{-1}. The net result was a slight increase in greenhouse trapping with increasing sea-surface temperature of $dF_n/dT_s \approx -0.8$ W m^{-2} K^{-1}. For sea-surface temperatures of 291 to 300 K, between 70 and 90 W/m^2 of sea-surface emission was radiated through the troposphere to space. At $T_s > 300$ K, there was a marked increase in downwelling flux by as much as $dF_d/dT_s \approx 25$ W m^{-2} K^{-1} (considering the convective region from 144°W to 164°W). The effect was a large increase in greenhouse trapping with increasing sea-sur-

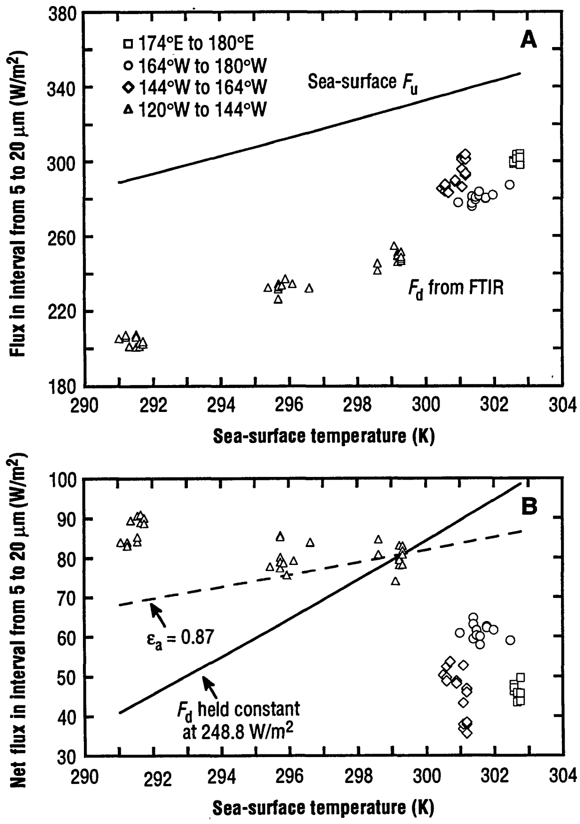

Fig. 4. Downwelling and upwelling (**A**) and net longwave fluxes (**B**) at the ocean surface, integrated over the spectral interval from 500 to 2000 cm^{-1}. Symbols in (A) denote downwelling flux F_d that was determined from the FTIR measurements, subdivided into the four longitude regions indicated. The solid line in (A) denotes upwelling Planck emission F_u from the ocean surface. The net $F_n = F_u - F_d$ is denoted by symbols in (B), again referring to the four longitude regions. The solid line in (B) denotes a hypothetical case in which the downwelling flux is held constant at 248.8 W/m^2. The dotted line in (B) denotes a hypothetical case in which the atmospheric emissivity (ε_a) (averaged over 500 to 2000 cm^{-1}) is held constant at 0.87 for all sea-surface temperatures.

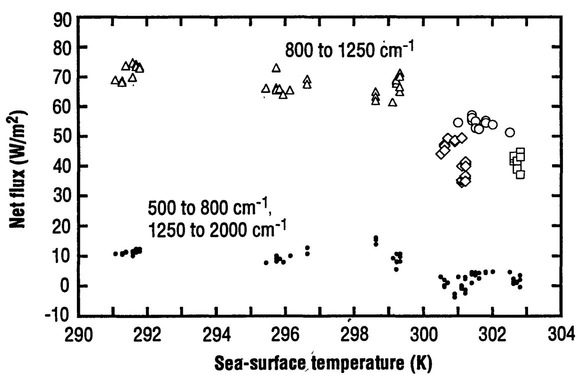

Fig. 5. Net flux at the ocean surface, determined from the FTIR measurements, integrated over the mid-IR window (800 to 1250 cm^{-1}) (denoted by the same symbols used in Fig. 4), and integrated over all measurable wave numbers outside the mid-IR window (denoted by solid points).

face temperature of $dF_n/dT_s \approx -19.5$ W m^{-2} K^{-1}. This is the super greenhouse effect as measured at the ocean surface, and its result was a net surface longwave flux from 35 to 55 W/m^2 for $T_s > 300$ K. If only the nonconvective warm pool region was considered, the net flux increased to 55 to 65 W/m^2 and $dF_n/dT_s \approx -7.5$ W m^{-2} K^{-1}.

I calculated a hypothetical net surface flux, assuming the downwelling flux $F_d = 248.8$ W/m^2, the value measured at 0405 UT on 24 March (12°N 138°E), where $T_s = 299.3$ K (Fig. 4B), to illustrate what would happen if the super greenhouse effect did not occur. It is conceivable that horizontal advection could remove sufficient energy or water vapor from the warm pool region to leave the atmosphere in nearly the same radiative state it is in when $T_s = 299$ to 300 K. If this were to happen, the net flux would increase slightly to around 90 W/m^2, meaning that surface emission would outpace greenhouse trapping. In this hypothetical case, there would be some mechanism by which energy is added to the warm pool region to raise the sea-surface temperature above 300 K, but this would only result in a greater longwave flux being radiated to space, and the warm pool region would be fundamentally stable against warming without the need for a climate thermostat. The FTIR data show a different situation—the super greenhouse effect results in a longwave back-radiation that increases nonlinearly with $T_s > 300$ K.

Alternatively, in the atmosphere, mid-IR emissivity could remain constant for all sea-surface temperatures (Fig. 4B). For the measured downwelling flux of 248.8 W/m^2 on 14 March, and for the approximation that the troposphere radiates as a gray body at the 850-mbar temperature level (*19*), the wave number–averaged (500 to 2000 cm^{-1}) emissivity of the atmosphere may be estimated as $\epsilon_a = 0.87$. Holding this emissivity constant for all sea-surface temperatures has qualitatively the same effect as holding the downwelling flux fixed. Surface emission outpaces greenhouse trapping, with net surface flux above 80 W/m^2 at the highest sea-surface temperatures.

The spectral resolution of the FTIR data confirms that the super greenhouse effect occurs primarily in the mid-IR window. In the warm pool region, net flux outside the interval from 800 to 1250 cm^{-1} is always less than 7 W/m^2 (Fig. 5), and the nonlinear increase in greenhouse trapping is due to emission from the H_2O continuum within the interval. Outside the warm pool region, net flux outside the spectral interval from 800 to 1250 cm^{-1} increases slightly to just above 10 W/m^2 as a result of a combination of lower surface air temperatures and slightly less saturation of water vapor rotation lines at wave numbers $\nu < 800$ cm^{-1}. These FTIR measurements therefore demonstrate the dominant role of the H_2O continuum in establishing the super greenhouse effect and its resulting back-radiation, which adds energy to the ocean surface. In addition to the quadratic increase in H_2O continuum opacity with increasing partial pressure of water vapor, the spectral interval from 800 to 1250 cm^{-1} is relatively transparent. Hence, an increase in opacity leads to a substantial increase in atmospheric emissivity.

To interpret these FTIR measurements in terms of the atmospheric greenhouse effect, one must compare the observed reductions in surface cooling with observations of longwave energy trapped by the atmosphere as measured at or above the tropopause. Analysis of 5 years of data from the Earth Radiation Budget Experiment (*20*) along the lines of Ramanathan and Collins (*4*), for the month of March and for clear-sky longwave measurements over the Pacific Ocean between 10°N and 10°S, shows a mean slope $dG_a/dT_s \approx 7.4$ W m^{-2} K^{-1}. During the time of the CEPEX study, $dG_a/dT_s \approx 10$ W m^{-2} K^{-1} (*9*). For all warm pool atmospheres sampled by the FTIR spectroradiometer, the mean slope $dF_n/dT_s \approx -8.4$ W m^{-2} K^{-1}, which is slightly larger than the climatological top-of-atmosphere mean from the Earth Radiation Budget Experiment. If only the nonconvective region (180°W to 164°W) is considered, $dF_n/dT_s \approx -7.5$ W m^{-2} K^{-1}, which is comparable to the top-of-atmosphere mean. If both convective regions sampled by the FTIR spectroradiometer are considered, $dF_n/dT_s \approx -10.1$ W m^{-2} K^{-1}; and if only the later convective region (164°W to 144°W) is considered, $dF_n/dT_s \approx -19.5$ W m^{-2} K^{-1}. Therefore, dF_n/dT_s determined from the FTIR measurements has at least the same magnitude as the climatological dG_a/dT_s measured from the top of the atmosphere; and where deep convection is present, dF_n/dT_s is generally larger than dG_a/dT_s measured at the tropopause during the same experiment. Hence, these FTIR measurements suggest that the super greenhouse effect contributes substantially to sea-surface heating.

REFERENCES AND NOTES

1. These experiments are the Tropical Ocean Global Atmosphere Coupled Ocean-Atmosphere Response Experiment (TOGA COARE) [P. J. Webster and R. Lukas, *Bull. Amer. Meterol. Soc.* **73**, 1377 (1992)] and CEPEX. The CEPEX Experiment Design Document is available from the Center for Clouds, Chemistry, and Climate, Scripps Institution of Oceanography, La Jolla, CA. CEPEX was conducted between 7 March and 7 April 1993 and deployed airborne and ship-based instruments to measure radiation fluxes, water vapor distribution, and evaporation from the sea surface. The primary goal of CEPEX was to test the thermostat hypothesis of sea-surface temperature regulation.
2. R. E. Newell, J. W. Kidson, D. G. Vincent, G. J. Boer, *The General Circulation of the Tropical Atmosphere and Interactions with Extratropical Latitudes* (MIT Press, Cambridge, MA, 1972), vol. 1.
3. D. E. Waliser *et al.*, *J. Clim.* **6**, 331 (1993).
4. V. Ramanathan and W. Collins, *Nature* **351**, 27 (1991).
5. T. H. Vonder Haar, in *Surface Radiation Budget for Climate Applications*, J. T. Suttles and G. Ohring, Eds. (NASA Ref. Publ. 1169, NASA, Greenbelt, MD, 1986), pp. 87–101.
6. The atmospheric greenhouse effect, G_a, is usually defined as the difference between the infrared flux emitted by the surface and the upwelling infrared flux at the top of the atmosphere (TOA), $G_a = \sigma T_s^4 - F_u$ (TOA). Thus, G_a refers to the net longwave energy absorbed (or trapped) by the atmospheric column.
7. A. Raval and V. Ramanathan, *Nature* **342**, 758 (1989).
8. R. Hallberg and A. K. Inamdar, *J. Clim.* **6**, 920 (1993).
9. F. P. Valero *et al.*, *Eos* **74**, 109 (1993).
10. The spin-up time required for convective activity to develop and that for horizontal advection are both approximately 2 weeks.
11. W. L. Smith *et al.*, *J. Atmos. Sci.* **50**, 1708 (1993).
12. D. Lubin, *J. Clim.* **7**, 121 (1994).
13. ______ and A. S. Simpson, *Geophys. Res. Lett.* **21**, 37 (1994).
14. H. E. Revercomb *et al.*, *Appl. Opt.* **27**, 3210 (1988).
15. The conversion factor, as a function of wave number, was estimated by use of the MODTRAN 2 radiative transfer model [A. Berk *et al.*, *MODTRAN: A Moderate Resolution Model for LOWTRAN 7* (Air Force Geophysics Laboratory GL-TR-89-0122, Hanscom AFB, MA, 1989)] to generate radiance spectra at the Gaussian quadrature angles [S. Chandrasekhar, *Radiative Transfer* (Dover, New York, 1960)]. These radiances were then integrated over angle to obtain the spectral downwelling flux. A subsequent MODTRAN 2 estimation of the zenith radiance then established the conversion factor. In the fully opaque parts of the mid-IR spectrum (650 to 700 cm^{-1}, 1350 cm^{-1}, and longer), the conversion factor was simply π. In the mid-IR region and in the region of H_2O vapor rotation lines (500 to 650 cm^{-1}), the conversion factor became increasingly greater than π as atmospheric opacity decreased. The conversion factor is therefore a function of wave number, atmospheric temperature, and water vapor abundance. With the sea-surface temperature and radiosonde data from the *Vickers*, MODTRAN 2 was used to generate conversion-factor spectra as a function of sea-surface temperature. On the basis of post-season inspection of the FTIR spectroradiometer's radiometric calibration, uncertainties in (wave number–integrated) downwelling flux estimated in this manner were ±3.0 W/m^2 for the mid-IR window region and ±6.0 W/m^2 for the measurable longwave region (500 to 2000 cm^{-1}).
16. The mean column abundances of water vapor, obtained from the *Vickers* rawindsondes, were 5.56, 4.19, 4.95, and 2.80 precipitable cm for the regions 174°E to 180°E, 180°E to 164°W, 164°W to 144°W, and 144°W to 120°W, respectively. Standard deviations were 0.47, 0.39, 0.50, and 0.98 cm, respectively.
17. L. S. Rothman *et al.*, *Appl. Opt.* **26**, 4085 (1987).
18. MODTRAN 2 calculations showed that thermal infrared wavelengths outside this region are dominated by water vapor emission bands that are mostly opaque and, at sea-surface temperatures greater than 299 K, would always add a constant 120 W/m^2 to the FTIR flux estimate.
19. *U.S. Standard Atmosphere Supplements, 1966* (Government Printing Office, Washington, DC, 1966).
20. E. F. Harrison *et al.*, *J. Geophys. Res.* **95**, 18,687 (1990).

21. Supported by NSF and by U.S. Department of Energy funds to the CEPEX project. The FTIR apparatus was developed with funding from the California Space Institute. I thank V. Ramanathan (Scripps Institution of Oceanography) for inviting participation in CEPEX and the officers and crew of the R.V. *John Vickers* for shipboard support.

8 February 1994; accepted 16 May 1994